Supplementary Information for "Orbital-selective charge-density wave in $TaTe_4$"

Supplementray Note 1: The Raman scattering spectra

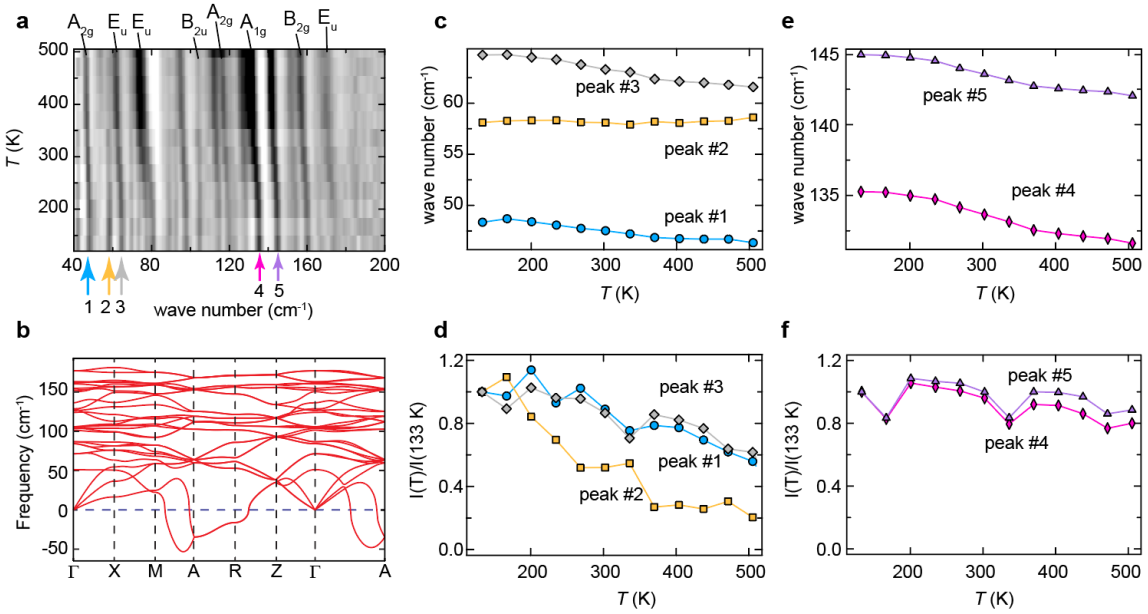

Supplementary Figure 1. a False-color plot of the temperature evolution of Raman spectra of $TaTe_4$. **b** Calculated phonon spectrum of $TaTe_4$ at temperature of 580 K. **c** Positions of the three low-energy peaks #1-3 as marked by the arrows in **a** as a function of the temperature. **d** Suppression of the intensity of peaks #1-3 with increasing temperature. The intensity of each peak was divided by its value at 133 K. **e**, **f** The same as **c** and **d** but for the peaks #4 and #5.

Supplementary Fig. 1 shows the Raman scattering spectra at selected temperatures. In general, most of the Raman peaks shift to lower energies and the intensities decrease with increasing temperature, as exemplified by the peaks #1, #3, #4, and #5 in Supplementary Figs. 1c-f. It's worth to note that the position of the peak #2 at 58 cm^{-1} shows a minor temperature dependence but its intensity is suppressed the most among all the Raman peaks (Supplementary Figs. 5c and d). The fitting of the peaks suggests that the intensity of the peak #2 at 58 cm^{-1} reduces by about 80% compared to about 40% (20%) for the peaks #1 and #3 (#4 and #5). The significant suppression and minor shift with increasing temperature suggest that this mode may be related to the CDW transition.

Supplementary Fig. 1b shows the calculated phonon spectrum in the normal state (the calculation of the phonon spectrum in the CDW state is not practical due to the complicated crystal structure),

which is consistent with previous result[1]. We note the phonon softening manifested by the imaginary phonon frequencies, which was attributed to the electron-phonon interaction instead of Fermi surface nesting in previous result[1]. It seems that the phonon frequencies in the Raman experiment approximate to the calculated phonon frequencies near the Γ point. Table 1 identifies the symmetry of the phonon modes and compares their frequency in the experiment and calculation. It is noteworthy that the measured phonon mode near 58 cm^{-1} that is suppressed the most at high temperature was not present in the calculation, supporting its intimate relationship with the CDW formation.

Supplementary Table 1. Comparison between the experimental and calculated phonon frequencies. Experimental results are measured at 133 K.

Mode	A_{2g}		E_u	E_u	B_{2u}	A_{2g}	A_{1g}	A_{1g}	B_{2g}	E_u
Exp (cm^{-1})	48.1	58.4	64.6	81.0	104.7	121.6	135.5	144.8	160.2	175.1
Cal (cm^{-1})	52.1		71.4	84.2	104.5	124.0	136.3	150.5	160.23	177.0

Supplementray Note 2: Comparison between experimental and calculated band structures along $\overline{\Gamma Z}$

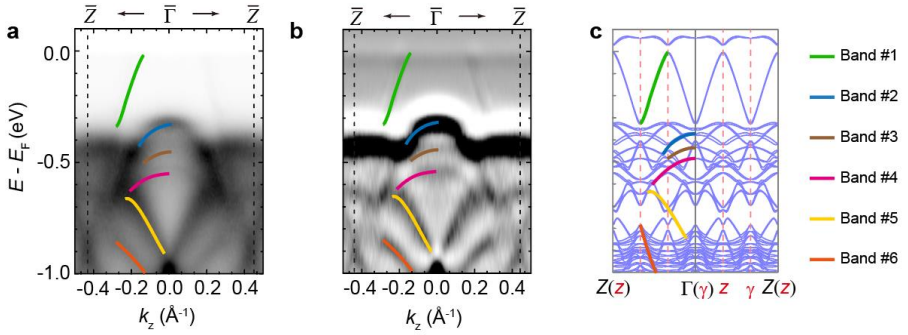

Supplementary Figure 2. Comparison between the experimental and calculated band structures along $\overline{\Gamma Z}$. **a** ARPES intensity map of the band dispersion along $\bar{\Gamma}\bar{Z}$. **b** Second derivative of the spectra in **a** with respect to the energy. **c** Calculated band structure along $\bar{\Gamma}\bar{Z}$. The bands #1-6 that can be resolved in the experiment are highlighted by thick colored lines.

The experimental band structure of $TaTe_4$ is in overall consistence with the density-functional theory (DFT) calculation in the 2×2×3 CDW state but much more complicated than the calculation in the normal state. Supplementary Fig. 2 compares ARPES measured band dispersions along $\overline{\Gamma Z}$ with the calculation. The measured bands #1-#6 are captured by the calculation although some of the folded bands and CDW gaps at high binding energies are not observed in the experiment.

Supplementray Note 3: The band sturcutre of the in-gap states

Supplementary Fig. 3 shows the band structure of the in-gap states. The band folding of the in gap states due to the 2×2×3 CDW formation induces an eye-shaped electronic pocket in ARPES intensity map in the k_x-k_z plane as marked by the red arrow in Supplementary Fig. 3a, consistent with the results in previous work[2]. The zoom-in plot of the band dispersion of the in-gap states in Supplementary Fig. 3b evidences the modulation of the band structure by the 3-fold CDW ordering along $\overline{\Gamma Z}$, which is well captured by the calculation in Supplementary Fig. 2c. Moreover, the dispersion of the in-gap states along $\bar{\Gamma}\bar{X}$ show a periodicity that is consistent with the reconstructed Brillouin zone (Supplementary Figs. 3c and d), also implying the CDW modulation effects.

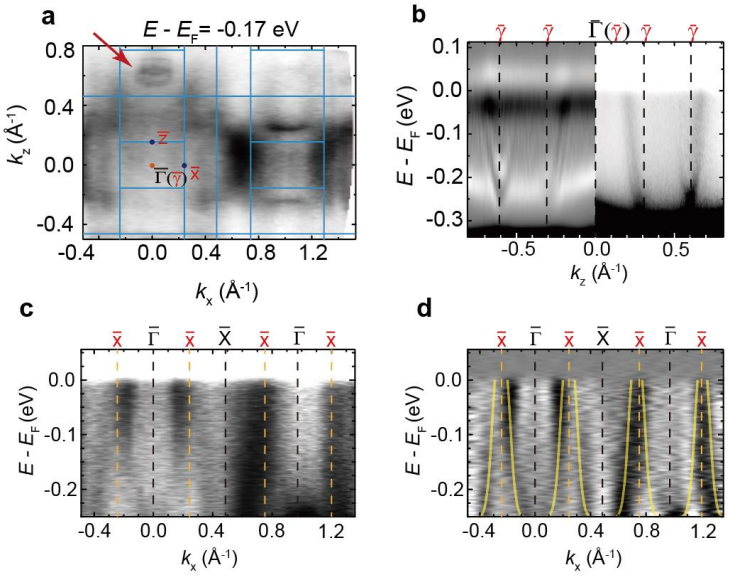

Supplementary Figure 3. The band dispersion of in-gap state. **a** ARPES intensity map at 0.17 eV below the Fermi level (E_F) in the k_x-k_z plane. **b** Dispersion of the in-gap states along $\bar{\Gamma}\bar{Z}$. The right and left of the panel **a** are ARPES spectra and its second derivative with respect to the energy. **c,d** ARPES spectra of the in-gap states along $\bar{\Gamma}\bar{X}$ (**c**) and its second derivative with respect to the energy (**d**). Data were collected using 24.8 eV photons at 40 K.

Supplementray Note 4: The chemical potential difference between experiment and calculation.

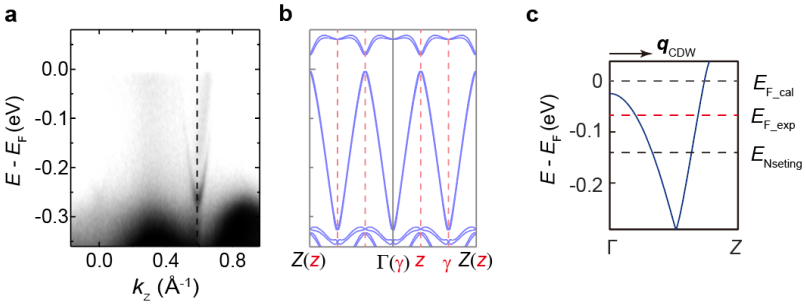

Supplementary Figure 4. Comparison between the experimental and calculated band structure. **a** ARPES intensity map of the in-gap states $\bar{\Gamma}\bar{Z}$. **b** Calculated band structure of the in-gap states in the CDW state. **c** Calculated band structure along ΓZ in the normal state.

In the main text, we argue that the calculation of the band structure in the normal state suggests the irrelevance of the Fermi surface nesting in the CDW transition, which neglects the difference

between the chemical potential in the experiment and calculation. This difference can be estimated by comparing the experimental and calculated band structure. Supplementary Fig. 4 suggests an insignificant difference between the chemical potential in the experiment and calculation. Supplementary Figs. 4a and b compare the band dispersion of the in-gap states. By comparing the measured and calculated band bottom of the in-gap states, we can estimate the difference in the chemical potential is about 65 meV. Assuming that the chemical potential does not change too much with temperature and a weak electronic correlation effect, we can then determine the "real" chemical potential in the calculation of the normal-state band structure, which is indicated by the red dashed line in Supplementary Fig. 4c. The Fermi surface nesting is still not satisfied after the chemical potential is aligned to the experimental value. The chemical potential needs to shift downwards by about 150 meV for the Fermi surface nesting condition to be satisfied (indicated by E_{Nesting} in Supplementary Fig. 4c). Therefore, the calculation indeed suggests the irrelevance of the Fermi surface nesting in the CDW transition.

Supplementray Note 5: The determination of the k_y position and the inner potential

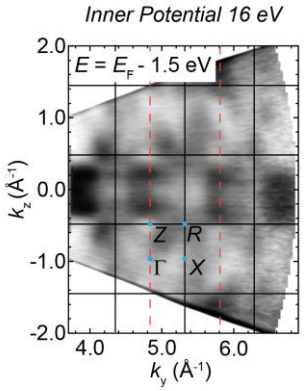

Supplementary Figure 5. k_y-k_z intensity map at -1.5 eV. Data was collected at 40 K using linear-horizontally polarized photons from 44 eV to 170 eV.

The k_y position can be determined by the periodicity of the ARPES intensity map in the k_y-k_z plane. Supplementary Fig. 5 shows the photon-energy dependent measurement of the constant-energy-contour at 1.5 eV below E_F. The ARPES intensity shows periodic distribution along k_y, which fits to the Brillouin zone with an inner potential of 16 eV.

Supplementray Note 6: Temperature evolution of band structure of $TaTe_4$.

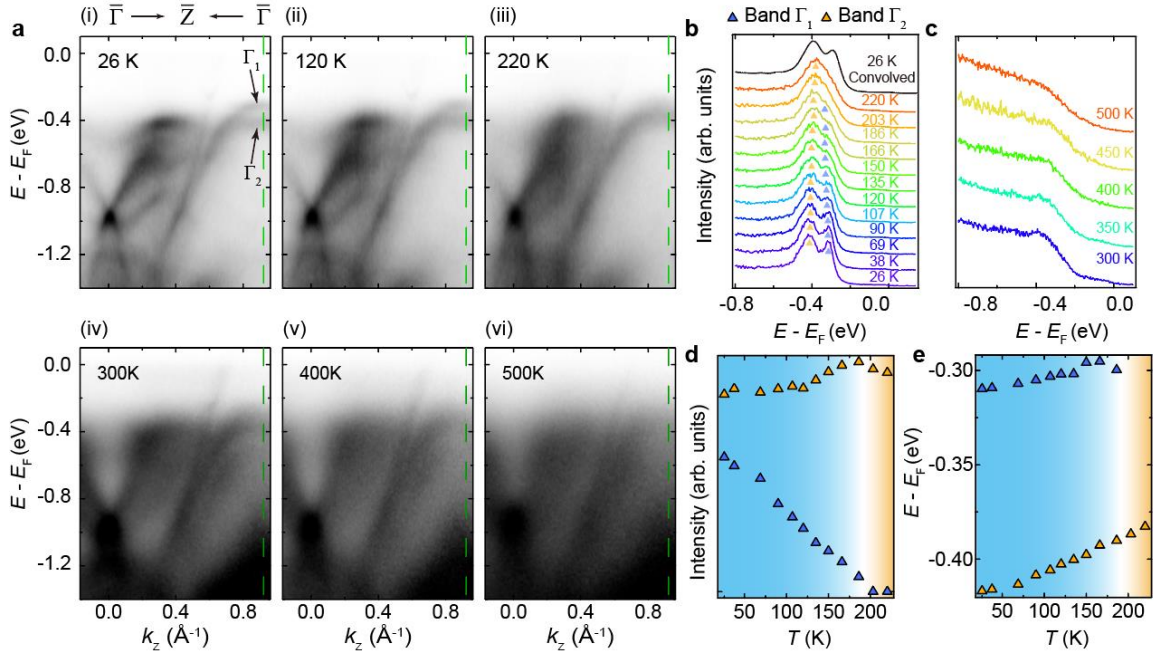

Supplementary Figure 6. Temperature evolution of the electronic structure of $TaTe_4$. a Band structure along the $\bar{\Gamma}\bar{Z}$ direction at selected temperatures. **b-c** Temperature evolution of energy distribution curves (EDCs) at k_z = 0.91 Å^{-1} ($\bar{\Gamma}$) marked by green dash lines in **a**(i-vi). Black line shows the EDC at 26 K convolved by Gaussian with width of 75 meV (4 times of k_BT at 220 K). **d-e** Peak intensity (**d**) and energy position (**e**) of the Γ_1 and Γ_2 bands extracted by fitting the EDCs to Lorentzians. Data below 300 K were collected using 24.8 eV photons and data above 300 K were collected using 21.2 eV photons delivered by a helium lamp.

To experimentally investigate the temperature dependence of CDW-modulated band structure, we measure ARPES spectra of $TaTe_4$ along $\bar{\Gamma}\bar{Z}$ in a large temperature range from 26 to 500 K, as shown in Supplementary Figs. 6a(i-vi). Please note that the data below and above 300 K were measured on different samples with different ARPES facilities. High-temperature meaurement were conducted using a helium lamp. We observe an inconspicuous change of the band structure with temperature. At the $\bar{\Gamma}$ point, the two bands Γ_1 and Γ_2 gradually approach each other and there is only one band above about 190 K, which is better visualized by the energy distribution curves in Supplementary Figs. 6b and 6c. We fit the EDCs at $\bar{\Gamma}$ to Lorentzians with the peak intensity and position of the Γ_1 and Γ_2 bands plotted as a function of temperature in Supplementary Figs. 6d and 6e. The EDC peak can be fitted by two and one Lorentzians below and above 190 K. It is worth to

note that the fit of the EDC peak to a single Lorentzian above 190 K cannot be explained by the thermal broadening effect (Supplementary Fig. 6b). The CDW gap persists up to 500 K, which may be due to the $\sqrt{2} \times \sqrt{2} \times 3$ CDW at high temperatures.

Supplementray Note 7: Surface doping evolution of band structure of $TaTe_4$.

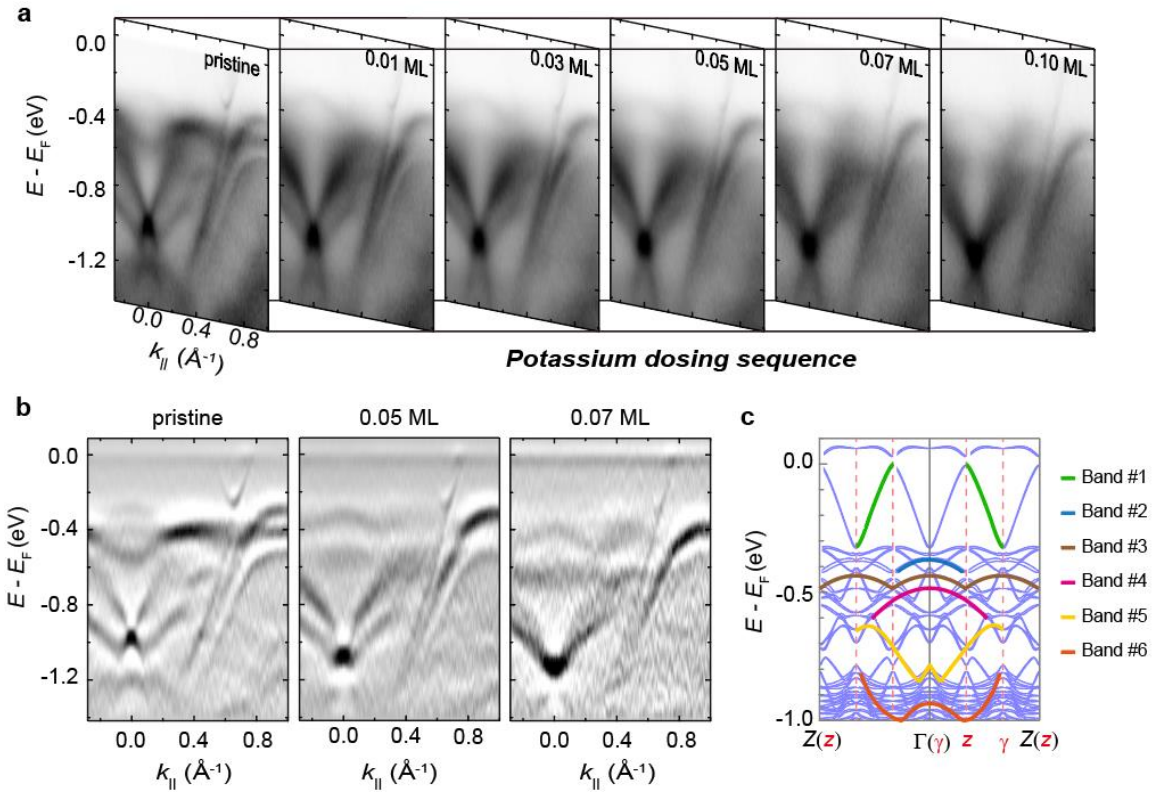

Supplementary Figure 7. Surface doping evolution of band structure of $TaTe_4$. a Evolution of the electronic structure of $TaTe_4$ with surface potassium doping. **b** Second derivative of the spectra at selected K doping level. Data were collected at 65 K using photon energies of 21.2 eV. **c** Calculated band structure along ΓZ in the CDW state. The coloured thick lines are the guides to eyes for the selected bands that are resolvable in the experiment (also see Supplementary Fig. 3).

The band structure evolution with increasing temperature implies the possible suppression of CDW long-range order. Hence, we conduct the surface potassium doping experiment to check its possible surface origin, shown in Supplementary Fig. 7. With increasing doping level, the bands shift towards higher binding energies. Moreover, the band #3 (Γ_2) is gradually suppressed and finally disappears at the doping level above 0.03 monolayer (ML) coverage. The band #4 was strongly

suppressed at the doping level of 0.1 ML. By comparing with our ab-initio calculation (also see the band comparison in Supplementary Fig. 3), we identify bands #3 (Γ_2) and #4 as CDW folded bands. Thus the surface doping evolution of the band structure suggests a suppression of CDW long-range order.

Supplementary Reference

1. Liu, F.-H., Fu, W., Deng, Y.-H., Yuan, Z.-B. & Wu, L.-N. First-principles study of the Kohn anomaly in $TaTe_4$. *Appl. Phys. Lett.* **119**, 091901, (2021).
2. Zhang, Y. *et al.* Charge order in a nonsymmorphic topological crystal $TaTe_4$. *arXiv preprint arXiv:2304.00425*, (2023).